SARTA CLOUDY : A Fast Forward Model which includes effects of cloud and aerosol scattering

S. De Souza-Machado[a], L. L. Strow[a],
S. E. Hannon[a]
[a] University of Maryland Baltimore County, Baltimore, MD 21250 USA

March 1, 2013

Abstract

The *sarta scatter* code is a modification of the UMBC clear sky *sarta* code, allowing users to compute synthetic infrared radiances for the AIRS instrument, in the presence of clouds and aerosols. By re-parameterizing the cloud scattering parameters into effective optical depths, the effect of clouds on upwelling radiation from the Earth's atmosphere is effectively recast as that of (an) additional absorbing gas(es), which allows us to use the efficient radiative transfer algorithm of the clear sky code. The liens of the code are that model vertical cloud fields (from eg ECMWF) need to be reshaped into at most two slab clouds. However, comparisons against packages which uses sophisticated algorithms (eg maximal overlap clouds and scattering trained on DISORT algorithm) shows that the *sarta scatter* code produces radiances accurate to about 3K (converted to equivalent Brightness Temperature)

1 Monochromatic Clear sky Radiative transfer algorithm

As a monochromatic beam of radiation propagates through a layer, the change in diffuse beam intensity $R(\nu)$ in a plane parallel medium is given by the standard Schwartschild equation [1, 2, 3]

$$\mu \frac{dR(\nu)}{dk_e} = -R(\nu) + J(\nu) \tag{1}$$

where μ is the cosine of the viewing angle, k_e is the extinction optical depth, ν is the wavenumber and $J(\nu)$ is the source function. For a non-

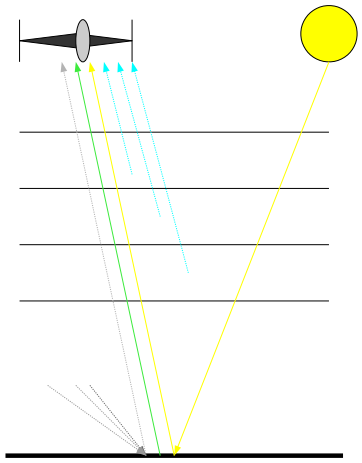

Figure 1: Illustration of contributions to measured Top Of Atmosphere radiance : (blue) layer emission, (green) surface, (yellow) solar and (gray) background thermal

scattering "clear sky", the source function is usually the Planck emission $B(\nu, T)$ at the layer temperature T, leading to an equation that can easily be solved for an individual layer. Dividing the atmosphere into layers and propagating the solution through the layers, the final radiance (for a downlooking instrument) can be written in terms of four components :

$$R(\nu) = R_s(\nu) + R_{layeremission}(\nu) + R_{th}(\nu) + R_{solar}(\nu) \qquad (2)$$

which are the surface, layer emissions, downward thermal and solar terms respectively. The terms in the equation are relatively straightforward, and the resulting algorithm is usually quite efficient.

Our monochromatic code kCARTA indexes the atmosphere so that layer 1 is the bottom and N (=100) the uppermost. Denoting $B(T)$ as the Planck function, T_s as the skin surface temperature, ϵ_s as the surface emissivity, θ as the satellite viewing angle, θ_{solar} as the sun zenith angle, $\tau_i(\nu)$ as the transmission of layer j ($\tau_i(\nu) = exp^{-k_i(\nu)}$), $\tau_{j\rightarrow m}(\nu)$ as the transmission from layer i to layer m, the individual terms are computed in monochromatic codes, such as kCARTA as follows.

1.1 Surface emission

This is simply the emission from the surface (temperature T_s), multiplied by the surface emissivity ϵ_s to account for the surface not being a perfect black body, and attenuated by absorption due to the atmosphere.

$$R_s(\nu) \quad = \quad \epsilon_s B(\nu, T_s)\tau_{1\to N}(\nu, \theta)$$

1.2 Layer emission

As the radiation emitted from the surface propagates up, it is absorbed by the layer of gas above it, and then re-emitted. This atmospheric emission happens layer by layer :

$$R_{layeremission}(\nu) \quad = \quad \sum_{i=1}^{i=N} B(\nu, T_i)(1.0 - \tau_i(\nu))\tau_{i+1\to N}(\nu, \theta))$$

Layers with negligible absorption ($\tau_i \to 1$) contribute negligibly to the overall radiance, while those with large optical depths ($\tau_i \to 0$) "black" out radiation from below. $(1.0 - \tau_i(\nu))$ is the emissivity of the layer while $(1.0 - \tau_i(\nu))\tau_{i+1\to N}(\nu, \theta))$ is the weighting function W_i of the layer.

1.3 Background thermal radiation

The atmosphere also emits radiation downward in a manner analogous to the upward layer emission just discussed. Upon reaching the surface, this radiance may be reflected upward. At the surface, the magnitude of this background term is :

$$R_{th}^{surface}(\nu) \quad = \quad \sum_{i=N}^{i=1} \int_0^{2\pi} d\phi \int_0^{\pi/2} d(cos\theta) cos\theta \rho(\theta, \phi) \times B(\nu, T_i) \times \Delta\tau \quad (3)$$

Here $\Delta\tau = (\tau_{i-1\to ground}(\nu, \theta) - \tau_{i\to ground}(\nu, \theta))$. Note the summation has been reversed, as we start out from the top of the atmosphere N, and come down to ground $i = 1$. This background thermal term also depends on the surface reflectivity ρ. If one assumes that the reflectivity of the surface is Lambertian, then ρ can be rewritten as $\frac{1-\epsilon_s}{\pi}$. This entire background reflected term is negligible in regions that are "blacked out," but in the window regions can contribute as much as 0.5 K of the total radiance when reflected back up to the top of the atmosphere.

Equation 3 involves an angular integration that needs to be done quickly but accurately. Layer by layer, the Mean Value Theorem means Eq. 3 can be rewritten in terms of an effective diffusive angle θ_d^i at each layer i :

$$R_{th}^{surface}(\nu) = \frac{1-\epsilon_s}{\pi}\frac{1}{2}\sum_{i=N}^{i=1} B(T_i)\left[\tau_{i-1\rightarrow ground}(\nu,\theta_{d1}^i) - \tau_{i\rightarrow ground}(\nu,\theta_{d2}^i)\right]$$

where based on the layer to ground transmissions of the $i, i-1$ th layers, $\theta_{d1}^i, \theta_{d2}^i$ are the optimum diffusion angles.

The value of θ_d^i that is often used is that of arccos(3/5) [1], especially for low optical depths ($k \leq 1$). A check of the accuracy of using this angle at all layers against an accurate computation using Eq. 3, showed that the errors in the window regions could be larger than 0.2 K, and would be even larger over land surfaces where the land surface emissivity is as low as 0.8. Instruments such as AIRS have channel radiance accuracies better than 0.2K, making it important to compute the background thermal correctly throughout the wavenumber region encompassed by the spectroscopic kCARTA database.

As Eq. 3 is computationally intensive, we devised the following. In an optically deep region, the surface is blacked out and one need not accurately compute the reflected term, and so arccos(3/5) can be used at all layers.

Conversely in an "optically thin" region, the layers closest to the ground contribute most to $R_{th}(\nu)$ (see discussion of weighting function above). For each 25 cm^{-1} region, the layer L above which arccos(3/5) can be safely used, was determined. Below this layer, we use a lookup table where θ_d^i angle is parameterized as a function of layer-to-ground optical depth (and hence transmittance).

With surface emissivity set at 0.8, L was chosen such that the brightness temperature errors at the top of the atmosphere were less than 0.1K for the sampling of profiles tested. The accuracy was checked by propagating the thermal background between the top of the atmosphere and the ground using this method, and comparing it to the results from using Eq. 3.

1.4 Solar radiation

Letting the solar reflectance be denoted by $\rho(\nu)$, then

$$\begin{aligned} R_{solar}(\nu) = {} & \rho(\nu)B_{solar}(\nu)cos(\theta_{solar}) \times \\ & \tau_{N\rightarrow ground}(\nu,\theta_{solar}))\tau_{ground\rightarrow N}(\nu,\theta))\Omega_{solar} \end{aligned}$$

ρ is usually (inaccurately) modeled as $\rho = \frac{1-\epsilon_s}{\pi}$. $\Omega_{solar} = \pi(r_s/d_{se})^2$ is the solid angle subtended at the earth by the sun, where r_e is the radius of the sun and d_{se} is the earth-sun distance. The solar radiation incident at the TOA $B_{solar}(\nu)$ comes from datafiles, and is modulated by the angle the sun makes with the vertical, $cos(\theta_{solar})$.

1.5 Monochromatic PCLSAM scattering algorithm

kCARTA can be interfaced with advanced scattering codes such as DISORT [4] and RTPSEC [5]. While well tested and numerically very accurate, these codes are complicated, leading to run times that can be significantly longer than for the clear sky case. In addition, the separation of radiative effects into solar and terrestrial means, for typical infrared instruments such as AIRS, IASI and CRiS, means one can optimize codes to work on either the thermal and/or the short wave infrared regions.

We chose to implement a fast code optimized to work where scattering is less important than absorption effects. In the thermal infrared, the effects of scattering due to aerosols and clouds is less than the effects of absorption, making the PCLSAM (Parameterization of Cloud Longwave Scattering for use in Atmospheric Models) scheme [6] very attractive. Since the model assumes the downward intensity through a cloud layer is the same as the Planck emission at the cloud temperature and thus simplifies the problem, it typically slightly overestimates the final TOA radiance. This algorithm changes the optical depth from k to a parameterized number $k\prime$ as described briefly below; more details can be found in [6, 7].

For each layer i that contains scatterers, we replace the optical depth with the total optical depth $k_{total}(\nu) = k_{atm}^{gases}(\nu) + k_{extinction}^{scatterer}(\nu)$. However this is reparameterized as

$$k\prime(\nu) = k_{total}(\nu) \times \{(1 - \omega(\nu)(1 - b(\nu))\}$$

where the effective single scattering albedo ω and backscatter b are obtained from the scatterer-only case ω_0 using

$$\omega(\nu) = \omega_0(\nu) k_{extinction}^{scatterer}(\nu)/k_{total}(\nu)$$

$$b(\nu) = (1 - g(\nu))/2$$

Note that if there are no scatterers in the layer, $\omega(\nu) \rightarrow 0$ and we recover the clear sky optical depth.

This same parameterization of the optical depth can be repeated for all the layers which contain scatterers, from which the radiative transfer

algorithm can be written in the same form as that for clear sky radiative transfer, with very little speed penalty. Since the scattering parameters $k_{extinction}^{scatterer}, \omega_0, g$ are stored in lookup tables as a function of particle size, it is trivial to obtain the derivatives with respect to size and particle amount. This method therefore immediately lends itself to be extended to compute scattering jacobians as well as fluxes, in a manner exactly analogous to that for clear sky jacobians and fluxes.

We have attempted to account for solar scattering in the SWIR, but comparing to DISORT and actual AIRS observations, we state this a significant lien on the code in this spectral region. We note that while computing the direct beam scattered solar contribution, we use the extinction optical depth k in $\left[1 - e^{-k(\frac{1}{\mu} + \frac{1}{\mu_{sun}})}\right]$, rather than the parameterized optical depth $k\prime$.

Some points to note are that

- While absorption spectra due to atmospheric gases has much structure, the crystal bonding, and smoothing over particle size distributions, "blurs" out sharp features, resulting in smooth absorption and scattering parameters.

- Aerosol particles range in size from 0.1 um (smoke) to 4 um (dust) in diameter, which means the thermal infrared is typically much more sensitive to dust than to smoke.

- Even for dust, non-sphericity of these particles is not a very big issue in the TIR. As long as realistic refractive indices are used, the results of Mie codes, integrated over realistic particle size distributions, should suffice to produce scattering parameters that can be relied upon.

- Similarly water clouds can be assumed to be spherical, typically 20 um in diameter.

- Cirrus can come in many different types of shapes or "habits", which typically depend on temperature through the height of the cloud. Since the resulting ice crystals can be quite large, whose shapes can deviate significantly from spherical, Mie codes should not be used to produce scattering parameters for use in terrestrial radiative transfer codes. We use cirrus scattering parameters for ice aggregates or hexagonal plates, provided by Anthony Baran of the UKMO.

2 SARTA Clear sky Radiative transfer algorithm

Keeping the surface and layer emission terms, while ignoring the solar and background thermal terms, the monochromatic clear sky radiative transfer algorithm can be written as

$$\begin{aligned} R_{toa}(\nu) &= \epsilon_s B(\nu, T_s)\tau_{1\rightarrow N}(\nu,\theta) + \\ &\quad \sum_{i=1}^{i=N} B(\nu, T_i)(1.0 - \tau_i(\nu))\tau_{i+1\rightarrow N}(\nu,\theta)) \\ &= \epsilon_s B(\nu, T_s)\mathcal{T}(\nu,\theta)^{1\rightarrow N} + \\ &\quad \sum_{i=1}^{i=N} B(\nu, T_i)\{\mathcal{T}(\nu,\theta)^{i+1\rightarrow N} - \mathcal{T}(\nu,\theta)^{i\rightarrow N}\} \end{aligned}$$

from which the top-of-Atmosphere radiance for an AIRS channel would be given by

$$R_{AIRS}(j) = \int_{\delta\nu_j} R_{toa}(\nu) SRF_j(\nu) d\nu$$

Notice that in both the surface term and the atmospheric emission term, we deal with layer to space transmittances, which means we need to take into consideration what is above each layer during the iteration of the radiative transfer algorithm. For a monochromatic code, this is not an issue, as Beer's law applies.

On a 2.3 GHz machine, a kCARTA run from 605-2830 cm^{-1} would take about 90 seconds, as optical depths have to be generated for about 900000 wavenumber points (spanning the above interval at 0.0025 cm^{-1} spacing) for each of the 100 layers. The spectral convolution for all 2378 channels using Matlab would add on an additional $\sim$ 10 seconds to generate one synthetic AIRS clear sky spectrum with the kCARTA line-by-line code.

With AIRS providing about 3 million spectra per day, it would clearly be next to impossible to use kCARTA in its current guise, to analyze the data. A fast Stand Alone Radiative Transfer Model (SARTA) was written, which takes a fraction of the above time (about 0.1 seconds) to generate one synthetic spectrum. For each AIRS channel, a simplified view of how this this code works is as follows. The atmospheric gas absorption for each layer of the channel in question is parameterized in terms of predictors such as layer temperature, gas absorber amounts (separated into water vapor,

ozone, other gases) and viewing angle geometry. A significant complication arises since we are dealing with layer to space transmittances, coupled with convolutions over finite channel widths. This leads to a breakdown in Beer's law. In other words, for example for two consecutive layers, if the monochromatic optical depth of each is $k(\nu)$) then, the transmittance from the bottom of one layer to the top of the next, is given monochromatically by

$$\tau_{\nu}^{i \rightarrow i+1} \quad = \quad exp(-k_i(\nu)) \;\; exp(-k_{i+1}(\nu))$$

In other words, at each wavenumber, the total transmittance through both layers, is the product of the transmittances through each layer

$$\mathcal{T}(\nu)^{i \rightarrow i+1} \quad = \quad \mathcal{T}(\nu)^{i} \;\; \mathcal{T}(\nu)^{i+1}$$

where $\mathcal{T}(\nu)^{l}$ is the monochromatic transmittance through layer l.

However, this law breaks down when looking at the convolved transmittance. For example, for AIRS channel j,

$$\tau_{airs}^{i \rightarrow i+1}(j) = \int_{\delta\nu_j} exp(-k_i(\nu)) \;\; exp(-k_{i+1}(\nu)) SRF_j(\nu) d\nu$$

which is NOT equal to

$$\int_{\delta\nu_j} exp(-k_i(\nu)) SRF_j(\nu) d\nu \;\; \int_{\delta\nu_j} exp(-k_{i+1}(\nu)) SRF_j(\nu) d\nu$$

ie

$$\mathcal{T}_{airs}^{i \rightarrow i+1}(j) \neq \mathcal{T}_{airs}^{i}(j) \;\; \mathcal{T}_{airs}^{i+1}(j)$$

When accounting for the convolved layer to space transmittance, not only does one have to consider the individual layers, but within each layer, the total optical depth is a sum over all contributing gases, further complicating matters. For example, for atmospheric layer i, the total monochromatic optical depth is due to a sum of contributions of all gases g such that

$$k_i(\nu) = k_i^{g1}(\nu) + k_i^{g2}(\nu) + ... + k_i^{gG}(\nu)$$

from which the transmittance is $\tau_i(\nu) = \Pi_{g=1}^{G} exp(-k_i^g(\nu))$. For AIRS channel j, the polychromatic transmittance required for a Fast Model is then

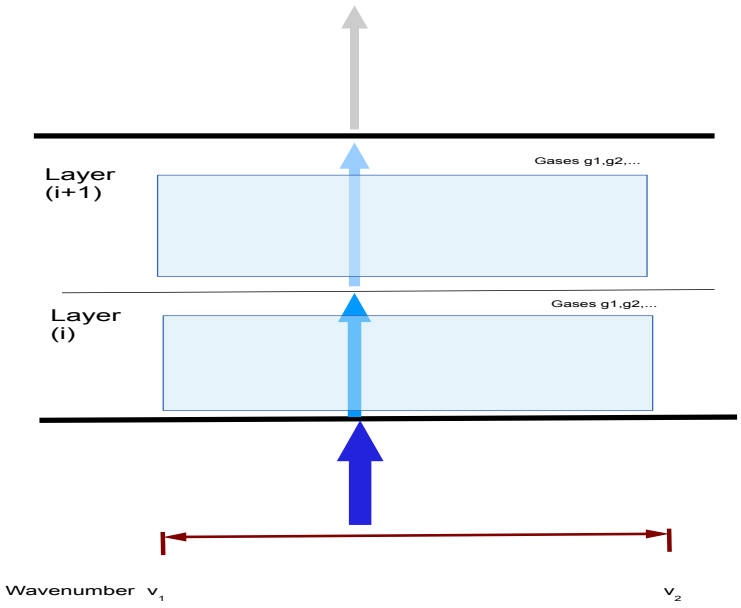

Figure 2: Pitfalls when applying Beer's law to finite width channels. Not only does it breakdown going from one layer to another, but in addition you cannot simply multiply in the contributions due to different gases

$\mathcal{T}^i_{airs}(j) = \int_{\delta\nu_j} \tau_i(\nu) d\nu$, and one immediately sees a breakdown of Beer's law within the individual layers!

In the making of a Fast Forward Model, monochromatic radiative transfer becomes polychromatic radiative transfer, and the above needs to be taken into consideration. This is especially so in the case when wants to be able to consider effects of individual variable gases such as ozone, water vapor, CO2 separate from the fixed gases. SARTA handles this problem by parameterizing effective layer to space transmittances, and then converting them to equivalent optical depths for each layer. Further details are given in [8, 9].

$$\begin{aligned} \mathcal{T}^{eff,i}_{airs}(j) &= \mathcal{T}^{i\rightarrow N}_{airs}(j)/\mathcal{T}^{i+1\rightarrow N}_{airs}(j) \\ \mathcal{OD}^{eff,i}_{airs}(j) &= -ln\{\mathcal{T}^{eff,i}_{airs}(j)\} \end{aligned}$$

This means that for each layer i and AIRS channel j, we have the effective optical depth due to atmospheric gases.

3 SARTA Cloudy/aerosol sky Radiative transfer algorithm

Recall from the earlier discussion on monochromatic scattering radiative transfer, the effects of clouds and aerosols was included by simply adding in the effective scattering optical depth. For the polychromatic case, we simply add on the effects of the relevant scatterer, where needed, and then perform the radiative transfer using the clear sky algorithm. The only time penalty incurred for each cloud/aerosol contaminated column of air, is reading in and interpolating the relevant scattering tables. Since the scattering parameters vary smoothly in spectral frequency, it is very straightforward to construct scattering optical depth tables for the jth AIRS channel for scattering species S; then for an arbitrary loading $q(j,i)^S$ g/m2

$$\begin{aligned} extinction(j,i,r)^S &= extinction(r)^S(1) \times q(j,i)^S \\ ssa(j,i,r)^S &= ssa(r)^S \\ g(j,i,r)^S &= g(r)^S \end{aligned}$$

where ssa and g are the single scattering albedo and asymmetry parameter respectively, and $extinction(j,r)^S(1)$ is the extinction for a column loading

of 1 g/m2; the particle size is denoted by r. The effective optical depths for channel j, layer i are then given by

$$k^{j,i}_{airs,total} = k^{j,i}_{airs}(gases) + extinction^{j,i}_{airs}(scatterer)$$

However again, to account for scattering effects, this is reparameterized as

$$kr^{j,i}_{airs} = k^{j,i}_{airs} \times \{(1 - \omega(j,i)(1 - b(j,i))\}$$

where the effective single scattering albedo ω and backscatter b are obtained from the scatterer-only case ω_0 using

$$\omega(j,i) = ssa(j,i) \times extinction(j,i)/k^{j,i}_{airs,total}$$

$$b(j,i) = (1 - g(j,i))/2$$

after which the radiance at top of the atmosphere can be calculated using the standard equations of radiative transfer.

4 Implementation details

Typically, Numerical Weather Prediction (NWP) models provide vertically resolved temperature and gas profiles at each grid point. Both kCARTA and SARTA ingest integrated versions of these profiles (via the associated *klayers* code), and use this information to compute optical depths which are then fed into the radiative transfer algorithm.

In addition, the NWP models also provide cloud fields at the same vertical resolution. When developing the SARTA-scatter code, we quickly realized that although liquid water and cirrus profiles were provided, as were total cloud fractions, we would run into an infinity of problems implementing cloud fractions, and in particular overlapping cloud fractions, at each AIRS layer. For this reason, we limit the SARTA-scatter code to having cloud/aerosol in at most *two* slabs. The input parameters for each of these slabs $k = 1, 2$ should include

- species (water cloud [101], ice (habit) cloud [201], or aerosol (type)[301])
- particle effective size (in um)
- loading (in g/m2); roughly for ice 50g/m2 = 1 OD, and for water 2g/m2 = 1 OD
- cloud/aerosol top (mb)

- cloud/aerosol bottom (mb)
- cloud fraction $0 \leq c(k) \leq 1$

In addition, we need a combined cloud fraction $C(k,l)$. For channel j the total radiance at the top of the atmosphere would then be

$$R_{AIRS}(j) = (1-(c(1)+c(2)-C(1,2))R_{clear}(j)+c(1)R^{(1)}_{cloud}(j)+c(2)R^{(2)}_{cloud}(j)$$

where $R_{clear}(j)$ is the radiance for a clear column of air, and $R^{(k)}_{cloud}$ is the radiance assuming a column of atmosphere completely filled with cloud of type $k = 1, 2$. Obviously if $c(1) = c(2) = C(1,2) = 0$ we get back a clear sky radiance. Depending on $c(k), k = 1, 2$ this means at worst, the cloudy sky code is about 3 times slower than the clear sky code.

One important point is what temperature the cloud is at, if it spans pressures (p1,p2) that is thicker than one AIRS layer, Need to look at the code!

4.1 Types of scatterers

We currently have scattering tables for a number of species. The tables span the full range of 2378 AIRS channels and a range of particle sizes; hence the scattering parameters for an arbitrary effective particle size is obtained by an interpolation. In addition the tables are for a particle loading of 1 g/m2; as explained above the extinction values for an arbitrary loading are obtained by a simple multiplication.

- aerosol (type 301)
  - desert dust
  - volcanic ash
  - effective diameter typically ranges from 0.5 to 10 um
- cirrus (type 201)
  - hex plates
  - aggregates
  - effective diameter typically ranges from 10 to 200 um
- water (type 101)
  - effective diameter typically ranges from 15 to 25 um

4.2 Cloud levels → slabs

As mentioned above, we need to go from $\simeq 90$ levels of cloud profile information, to two slabs. Our "emcwf2sarta" matlab routine does the necessary manipulations, summarized below.

4.2.1 Input requirements

As stated above, in addition to the usual temperature and trace gas profiles, we also need the following information from ECMWF/ERA

- p.ciwc : 91xP cloud ice profiles
- p.ciwc : 91xP cloud ice profiles
- p.cc : 91xP cloud total fraction

4.2.2 Smooth the input profiles

Normalize cloud profile eg
$normalized_{ice} = ice_{profile}(:, ii)/max(ice_{profile}(:, ii))$
Smooth normalized profile
$normalized_{ice} \rightarrow normalized_{ice}^{smoothed}$

4.2.3 Turn smoothed profile into slab profiles

Find how many peaks are present in this normalized profile, and "width" of peaks. The widths will help determine the cloud top and bottom
From above, start combining peaks so that we have at most two peaks for ice cloud, and two peaks for water cloud
Finally, combine so at most we have two slabs

4.2.4 Determine effective particle sizes, cloud amounts and cloud fractions

The cloud amount for each slab is then determined by converting the original ice/water cloud profile (in g/g) to integrated g/m2; the effective particle size for water is set to 20 um $\pm$ random amount, while for cirrus the particle size is set according to the temperature of the cloudtop (again, $\pm$ a random amount. Cloud fracs for each cloud, and the overlap, are randomly set (using the "cc" field), so that they satisfy

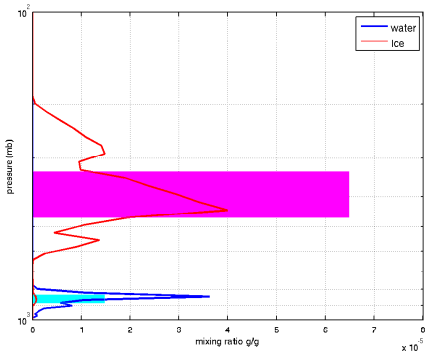

Figure 3:

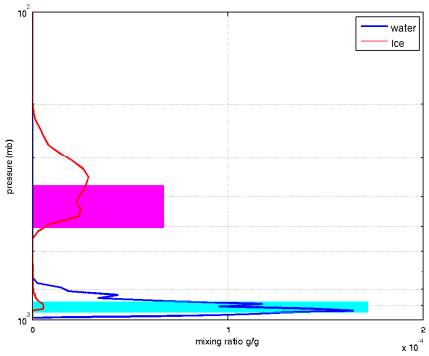

Figure 4:

- c(1) $\leq$ 1, c(2) $\leq$ 1
- c(1,2) $\leq$ min(c(1),c(2))
- clear = 1 - (c(1)+c(2) - c(1,2))
- c(1) exclusively = c(1) - c(1,2)
- c(2) exclusively = c(2) - c(1,2)

4.2.5 Examples

Figures 3-6 illustrate the results of our "emcwf2sarta" code. Blue and Red are the ECMWF 91 level water and ice profiles (in g/g) while cyan and magenta are the water and cirrus slabs we end up with. The horizontal extent of the slabs are the integrated cloud profiles, converted to g/m2 and normalized by a factor of 10000 for the plots. It is possible to tweak the "emcwf2sarta" code in the future. For example we can move the cirrus cloud higher, if we want to reduce overall computed radiances.

5 Comparison to AIRS observations

We have been able to make some comparisons of SARTA-scatter against AIRS observations, for the 10 years of data available to us. Figure 7 is a gridded map showing daytime AIRS 1231 cm^{-1} observations (converted to BT), while Figure 8 is a similar map, showing SARTA-scatter calculations, using ERA fields. Notice the overall similarities in the two figures. Obvious differences include the DCC clouds seen in the AIRS observations, and not

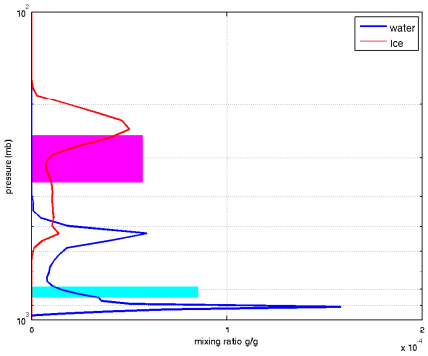

Figure 5:

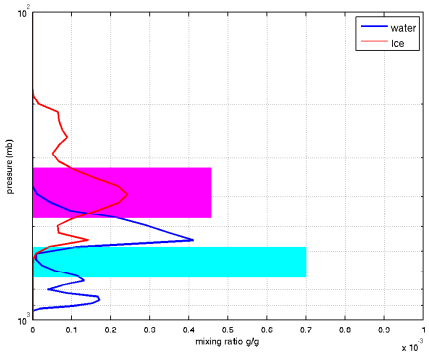

Figure 6:

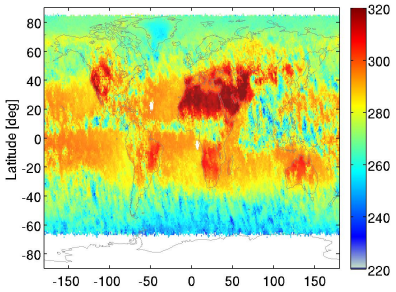

Figure 7: AIRS BT1231 cm^{-1} observations in July 2007

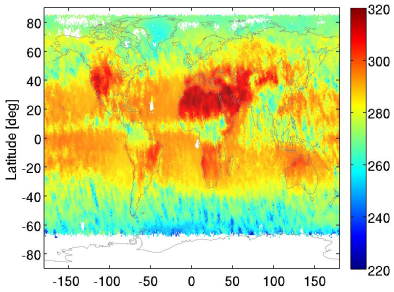

Figure 8: SARTA-scatter calculations for 1231 cm^{-1}, using ERA fields for July 2007

present in the calculations. Though not shown here, this problem is also seen when using ECMWF model fields. Since these maps are for July, no daytime AIRS observations are possible over the South Polar region.

The next two figures are a zoom in on the Pacific/Indian Oceans, for March 10,2011; the SARTA-scatter calculations used ECMWF fields, which are higher resolution in time and space. Figure 9 is a gridded map showing daytime AIRS 1231 cm^{-1} observations (converted to BT), while Figure 10 is a similar map, showing SARTA-scatter calculations. Notice the overall similarities in the two figures.

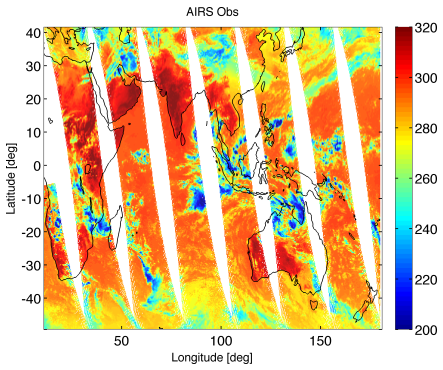

Figure 9: AIRS BT1231 cm^{-1} observations for March 11, 2011

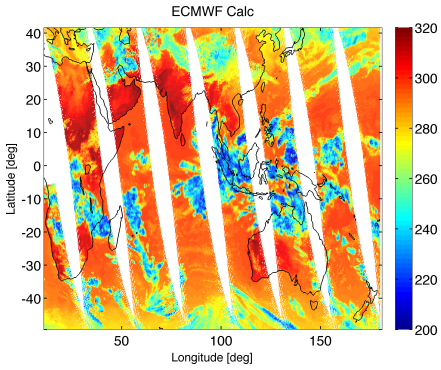

Figure 10: SARTA-scatter calculations for 1231 cm^{-1}, using ECMWF fields for March 11, 2011

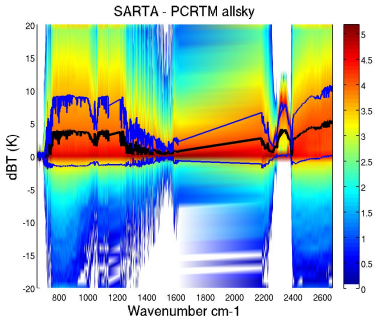

Figure 11: Comparing SARTA-scatter vs PCRTM

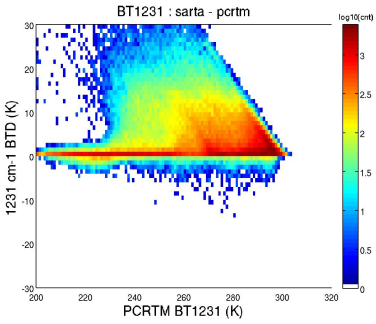

Figure 12: BT1231 comparisons

6 Comparison to more sophisticated algorithms

We have been able to make some comparisons of SARTA-scatter against PCRTM, which is a Fast Radiative Transfer code trained using DISORT. The implementation we compare against uses 50 random maximal overlap clouds. Other differences are that the PCRTM implementation uses ice cloud sizes that vary between 50 to 125 um, fixed 20 um water sizes, and Ping Yang's scattering parameters. The same ECMWF profiles were sent in for both SARTA-scatter and PCRTM, for nadir observations for May 2012.

Figure 11 is a 2d histogram, showing bias between the two codes as a function of wavenumber. The thick black line is the mean of the bias, while the blue lines are one standard deviation away; the colorscale is the log of

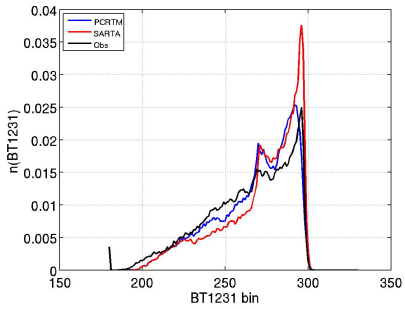

Figure 13: Comparing SARTA-scatter vs PCRTM vs AIRS observations, over all the globe

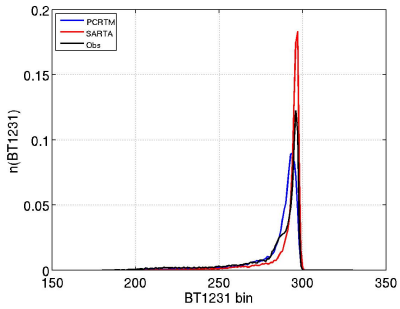

Figure 14: Comparing SARTA-scatter vs PCRTM vs AIRS observations, over the Tropical Pacific

the number of instances. The figure shows that typically SARTA-scatter produces brightness temperatures that are about 3 $\pm$ 4 K warmer than PCRTM, for window channels. This could arise from a number of factors, such as too little cirrus cloud (either amount or fraction). To alleviate this, it is possible to tweak our "emcwf2sarta" code, as mentioned in section 4.2.5. Figure 12 shows the BT1231 cm^{-1} bias between PCRTM and SARTA-scatter, as a function of computed PCRTM temperature. The colorscale is the log of the number of observations, and shows that the differences typically begin to manifest at about 260 K.

.

Figures 13 and 14 shows the BT1231 cm^{-1} pdfs over all points on the globe, and over the Tropical Pacific. In each case, blue, red and black are the PCRTM, SARTA-scatter and AIRS observations, respectively. As expected from the above discussion, typically SARTA-scatter is "warmer" than PCRTM, but it is not easy to chose between the two when comparing to the AIRS observations.

While the speeds of the two codes are very similar, the architecture of our SARTA-scatter is very much the same as the clear sky SARTA code, and so should be easy for a new user to learn. The user can use an ice cloud with more loading to bring the SARTA-scatter line more in line with the PCRTM simulations.In addition, and perhaps more correctly, the "ecmwf2sarta" routine should be easy to modify, in order to move cirrus clouds higher up, if we feel the radiances need to be made smaller. Alternately, Figures 15 and 16 shows the night time biases between SARTA-scatter and PCRTM for 820, 960, 1231 and 2616 cm^{-1} over all points on the globe. The graph on the left

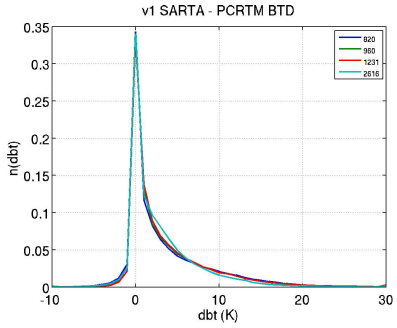

Figure 15: Comparing SARTA-scatter vs PCRTM (50 subcolumns)

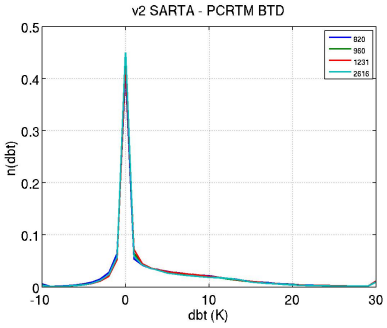

Figure 16: Comparing SARTA-scatter vs PCRTM (1 subcolumn)

uses the 50 subcolumn version of PCRTM while the one on the right shows a one subcolum version, and one sees that clearly the tail has been modified.

.

References

[1] K.N. Liou. *An Introduction to Atmospheric Radiation*. Academic Press, 1980.

[2] R.M. Goody and Yung. Y.L. *Atmospheric Radiation: Theoretical Basis*. Oxford University Press, 1989.

[3] D.P. Edwards. GENLN2: A general line–by–line atmospheric transmittance and radiance model. *NCAR Technical Note 367+STR*, National Center for Atmospheric Research, Boulder, Colo., 1992.

[4] K. Stamnes, S.-C. Tsay, W. Wiscombe, and K. Jayaweera. Numerically stable algorithm for discrete ordinate method radiative transfer in multiple scattering and emitting layered media. *Appl. Opt*, 27:2502–2509, 1988.

[5] M.N Deeter and F. Evans. A Hybrid Eddington Single Scattering Radiative Transfer Model for computing radiances from thermally emitting atmospheres. *JQSRT*, 60:635–648, 1998.

[6] M.-D. Chou, K.-T. Lee, S.-C. Tsay, and Q. Fu. Parameterization for cloud longwave scattering for use in Atmospheric Models. *J. Climate*, 12:159–169, 1999.

[7] M. Matricardi. RTIASI radiative transfer code for ECMWF, 2005. private communication.

[8] S.E. Hannon and L. L. Strow. SARTA: The stand-alone airs radiative transfer algorithm. Technical report, University of Maryland Baltimore County, Department of Physics, http://asl.umbc.edu/rta/sarta.html, 2002.

[9] L. Strow, S. Hannon, S. DeSouza-Machado, D. Tobin, and H Motteler. An overview of the AIRS radiative transfer model. *IEEE Transactions on Geosciences and Remote Sensing*, 41:303–313, 2003.